Supplementary Information for

The Oscillatory Photoelectron Signal of *N*-Methylmorpholine as a Test Case for the Algebraic-Diagrammatic Construction Method of Second Order

Raison Dsouza,[†] Xinxin Cheng,[†,‡] Zheng Li,[†] R. J. Dwayne Miller,[†,‡,¶] and Michał Andrzej Kochman[*,§]

[†] Max Planck Institute for the Structure and Dynamics of Matter, Bldg. 99 (CFEL), Luruper Chaussee 149, 22761 Hamburg, Germany.
[‡] Hamburg Centre for Ultrafast Imaging (CUI), Universität Hamburg, Luruper Chaussee 149, 22761 Hamburg, Germany.
[¶] Department of Chemistry and Physics, University of Toronto, 80 St. George Street, Toronto, Ontario M5S 3H6, Canada.
[§] Department of Physics, Chemistry and Biology (IFM), Linköping University, 581 83 Linköping, Sweden.

e-mail: michal.kochman@liu.se

1 Choice of model chemistry

As a preliminary to the present study, we concerned ourselves with the choice of appropriate model chemistry for the modeling of the relevant excited and ionized states of *N*-methylmorpholine (NMM). Presently, we provide a summary of our findings in this regard.

1.1 Basis set effects

As a rule, diffuse electronic states such as Rydberg-type excited states are demanding on the basis set, sometimes requiring multiple layers of diffuse basis functions. For this reason, our first order of business was to investigate basis set effects in the calculation of vertical excitation energies and vertical ionization potentials (VIPs) of NMM.

All calculations were performed at the chair-equatorial ground-state equilibrium geometry of NMM as optimized at the MP2 level of theory in combination with the r-aug-cc-pVDZ basis set ("reduced aug-cc-pVDZ"; see Section 2.1 of the main body of the present paper for a definition of that basis set).

The vertical excitation energies were calculated with the of equation of motion coupled-cluster method with single and double excitations[1] (EOM-CCSD) method,

Table S1: Basis set effects in the computation of the relevant excited and ionized states of NMM. Upper part: vertical excitation spectrum as calculated with the use of the EOM-CCSD method. Lower part: vertical ionization spectrum, calculated via the EOM-IP-CCSD method.

Excited states	State	Basis set		
		r-aug-cc-pVDZ	aug-cc-pVDZ	(d)-aug-cc-pVDZ
		ΔE, eV	ΔE, eV	ΔE, eV
	S_1 (3s)	5.787	5.785	5.745
	S_2 ($3p_z$)	6.245	6.237	6.148
	S_3 ($3p_x$)	6.276	6.276	6.207
	S_4 ($3p_y$)	6.485	6.471	6.385

Ionized states	State	Basis set		
		r-aug-cc-pVDZ	aug-cc-pVDZ	(d)-aug-cc-pVDZ
		VIP, eV	VIP, eV	VIP, eV
	D_0	8.414	8.438	8.440
	D_1	9.426	9.458	9.459

implemented in the program Molpro, version 2012.1.[2] EOM-CCSD is the highest-level approximation within the hierarchy of coupled cluster excited-state methods that we are able to apply to the relatively large NMM molecule. Previous studies by Szalay et al.[3] and Tajti and Szalay[4] have reported that the inclusion of triple excitations has only a slight effect (of the order of 0.1-0.2 eV) on calculated vertical excitation energies into Rydberg states. It follows that vertical excitation energies calculated with the use of the EOM-CCSD method should be reasonably close to converged with respect to the excitation level.

In turn, the VIPs were computed via the equations of motion ionization potential coupled-cluster[5,6] (EOM-IP-CCSD) method, available in the open-source Northwest Computational Chemistry Package (NWChem), version 6.6.[7]

Either calculation was performed with, firstly, the r-aug-cc-pVDZ basis set; secondly, the standard aug-cc-pVDZ basis set; and, thirdly, a mixed basis set which used aug-cc-pVDZ for the hydrogens, and the doubly augmented d-aug-cc-pVDZ basis set[8] for the heavy atoms. In what follows, we will denote this last-mentioned basis set (d)-aug-cc-pVDZ. In all cases, a RHF reference determinant was used, and the frozen core approximation was applied.

The results are presented in Table S1 above. As expected, increasing augmentation of the basis set with diffuse functions stabilizes the Rydberg-type excited states of NMM relative to the ground state, leading to a lowering of the vertical excitation energies. Fortunately, in the case of the S_1 (3s) state, this effect is rather weak: on going from the modestly augmented r-aug-cc-pVDZ basis set to the extensively augmented (d)-aug-cc-pVDZ basis set, the vertical excitation energy is only lowered by 0.042 eV. The 3p-type states turn out to be slightly more sensitive to the extent of augmentation, but even for these states, the

lowering of vertical excitation energies on going from r-aug-cc-pVDZ to (d)-aug-cc-pVDZ is only around 0.1 eV.

In turn, the calculated VIP values increase with increasing extent of augmentation, and this is true of both the D_0 and D_1 ionized states. This effect is presumably due to the fact that the electron density of the ground state of the neutral molecule, while relatively compact, is more diffuse than that of the radical cation. Hence, increasing extent of augmentation stabilizes the ground state of the neutral molecule relative to the radical cation. In absolute terms, however, this effect is small in magnitude.

In conclusion, basis set effects in the calculation of the relevant excited and ionized states of NMM are, on the whole, rather weak. Already the modestly augmented r-aug-cc-pVDZ basis set is sufficient to provide a realistic description of these states. A considerable saving of computing time can be achieved by performing electronic structure calculations with that basis set, as opposed to the larger aug-cc-pVDZ and (d)-aug-cc-pVDZ basis sets.

As a matter of fact, it seems that there is be little to be gained from applying a basis set larger than r-aug-cc-pVDZ when the excited and ionized electronic states of NMM are being calculated with the use of the MP2/ADC(2) combination. This is because, as will be discussed in the next section, the MP2/ADC(2) method itself gives rise to large systematic errors in the calculation of vertical excitation energies into diffuse excited states. This deficiency of MP2/ADC(2) arguably defeats the purpose of applying a high-quality basis set.

1.2 Assessment of ADC(2) for excitation energies and ionization potentials

Our choice of the MP2/ADC(2) combination for the description of the electronic structure of NMM was motivated in part by its low computational cost and excellent numerical stability. Both factors are of crucial importance for semiclassical simulation methods such as Born-Oppenheimer molecular dynamics (BOMD). Another advantage of MP2/ADC(2) for the purposes of the present study is the fact that ionized states and Dyson orbitals for ionization can be readily computed via the continuum orbital formalism.[9,10]

In this section, we evaluate the accuracy of MP2/ADC(2) for the relevant vertical excitation energies and vertical ionization potentials (VIPs) of NMM. Such an assessment is necessitated by the fact that the closely related second-order approximate coupled cluster[11–13] (CC2) method systematically underestimates vertical excitation energies into Rydberg-type states.[3,4] The reasons underlying this systematic error of CC2 were investigated in depth by Tajti and Szalay.[4] In the linear response formulation of CC2, the excitation energies are obtained as the eigenvalues of the CC2 Jacobian:

$$\mathbf{A}^{\mathrm{CC2}} = \begin{pmatrix} \langle \mathbf{S}|[H,\hat{\tau}_1]\exp(\hat{T}_2)|0\rangle & \langle \mathbf{S}|[H,\hat{\tau}_2]|0\rangle \\ \langle \mathbf{D}|[H,\hat{\tau}_1]|0\rangle & \mathbf{A_{DD}} \end{pmatrix} \tag{1}$$

Tajti and Szalay have demonstrated that the understimation of vertical excitation energies into Rydberg-type states is related to the diagonal structure of the $\mathbf{A_{DD}}$ block of the CC2 Jacobian:[4]

$$(\mathbf{A_{DD}})_{\mu\nu} = \delta_{\mu\nu}\,\omega_{\nu_2} \tag{2}$$

where ω_{ν_2} is the so-called excitation energy of determinant ν_2.

Methods such as ADC(2) and also the CIS(D_∞) model[14] introduced by Head-Gordon

and coworkers can be considered as derived via the modification of the CC2 Jacobian.[12] These methods retain the same diagonal form of the $\mathbf{A_{DD}}$ block. Therefore, by extrapolation, these methods can also be expected to suffer from the same systematic error for Rydberg-type states.

Moreover, we note that in the continuum orbital method, ionization is considered as the excitation of an electron from an occupied orbital localized on the molecule into an extremely diffuse virtual orbital, meaning that the ionized state is essentially treated as the limiting case of a Rydberg state. For this reason, MP2/ADC(2) is likewise expected to underestimate VIPs.

We elected to use the coupled-cluster calculations of the vertical excitation energies and VIP as the benchmark by which to assess the MP2/ADC(2) method. The upper part of Table S2 compares the vertical excitation energies obtained with the EOM-CCSD and the MP2/ADC(2) methods. As expected, for each of the lowest four excited states, MP2/ADC(2) underestimates the vertical excitation energy relative to the benchmark provided by the EOM-CCSD method. Of main interest to us is the S_1 (3s) state, for which the vertical excitation energy predicted by MP2/ADC(2) is 0.526 eV lower than that obtained with the more reliable EOM-CCSD method.

Moving now on to discuss the ionized states, the VIPs obtained with the two methods are listed in the lower part of Table S2. As in the case of the vertical excitation energies, the VIPs calculated with MP2/ADC(2) are strongly underestimated with respect to EOM-IP-CCSD, but the errors are even larger. In particular, MP2/ADC(2) underestimates the VIP of the D_0 state by as much as 0.919 eV relative to the EOM-IP-CCSD value.

Table S2: Benchmarking the MP2/ADC(2) combination against the coupled cluster methods. Upper part: vertical excitation spectrum – vertical excitation energies (ΔE) and associated oscillator strengths (f). Lower part: vertical ionization spectrum – vertical ionization potentials (VIPs).

Excited states	State	EOM-CCSD		MP2/ADC(2)	
		ΔE, eV	f	ΔE, eV	f
	S_1 (3s)	5.787	0.0127	5.261	0.0145
	S_2 ($3p_z$)	6.245	0.1329	5.703	0.0877
	S_3 ($3p_x$)	6.276	0.0072	5.729	0.0051
	S_4 ($3p_y$)	6.485	0.0158	5.900	0.0074

Ionized states	State	EOM-IP-CCSD VIP, eV	MP2/ADC(2) VIP, eV
	D_0	8.414	7.494
	D_1	9.426	8.272

It is inevitable that the errors in vertical excitation energies and ionization potentials calculated with the use of the MP2/ADC(2) method will propagate into the simulated TRPES spectrum. On the basis of the results of Section 2.4.3 of the main body of the present work, the electron binding energy (E_b) was calculated as the vertical energy difference between the D_0 and S_1 states. Accordingly, we may rewrite the expression for E_b in terms of the vertical ionization potential (VIP) of the D_0 state, and the vertical excitation energy into the S_1 state (ΔE) at a given nuclear geometry:

$$E_\mathrm{b} = E[\mathrm{D}_0] - E[\mathrm{S}_1] = \underbrace{(E[\mathrm{D}_0] - E[\mathrm{S}_0])}_{\mathrm{VIP}} - \underbrace{(E[\mathrm{S}_1] - E[\mathrm{S}_0])}_{\Delta E} \tag{3}$$

According to the benchmark provided by the coupled cluster methods, MP2/ADC(2) underestimates both the VIP and ΔE, but the former quantity is underestimated more strongly than the latter. As a consequence, there will be only partial error cancellation between the VIP and ΔE. By our best estimate, the VIP is underestimated by some 0.9 eV, and ΔE by roughly 0.5 eV (as a first approximation, we assume that these errors are independent of molecular geometry). It follows that the electron binding energy predicted by MP2/ADC(2) will be consistently underestimated by some 0.4 eV.

In the experimentally-observed TRPES spectrum of NMM, the signal from S_1 (3s) state occurs in the electron binding energy range of roughly 2.80 to 3.05 eV. The simulations reported in the main body of the present work place it in the range of 2.20 to 2.40 eV, some 0.6 eV lower. Thus, the actual error in the position of the signal (0.6 eV) coincides quite closely with our best theoretical estimate of the error (0.4 eV). This observation suggests that the inaccuracy of the MP2/ADC(2) method accounts for most of the error in the calculated position of the signal of the S_1 (3s) state. Presumably, other sources of error, such as basis set incompleteness, and the assumption that the probe pulse does not impart any energy on the nuclear wavepacket, are smaller in magnitude, leaving the inaccuracy of MP2/ADC(2) as the predominant source of error.

1.3 Assessment of ADC(2) for D_0-S_1 gradient difference vector

As discussed in Section 2.4.5 of the main body of the present paper, the sensitivity of the electron binding energy associated with the S_1 (3s) $\rightarrow$ D_0 photoionization process can be related to the gradient difference vector between the states D_0 and S_1 (3s). Therefore, it is also of interest to verify whether MP2/ADC(2) predicts a realistic gradient difference vector. To this end, the gradient difference vector was re-calculated with the use of coupled cluster methods. For the purpose of this benchmark calculation, we selected the chair-equatorial ground-state equilibrium geometry of NMM as optimized at the MP2/r-aug-cc-pVDZ level of theory.

These additional coupled cluster calculations were performed within the program PSI4, version 1.0.0,[15] which contains an implementation of analytic gradients for the CCSD and EOM-CCSD methods. Here, the S_1 (3s) state was treated with the use of the EOM-CCSD method applied with a RHF reference determinant. In turn, the D_0 state was accessed with the CCSD method in combination with a restricted open-shell Hartree-Fock (ROHF) determinant. Due to program limitations, in these calculations all electrons (including core electrons) were included in the correlation treatment. The 'no_reorient' and 'no_com'

keywords were used in order to prevent the reorientation of the molecule by the program.

Figure S1 compares the gradient difference vector from the coupled cluster methods with that obtained at the MP2/ADC(2) level. Visual inspection indicates that in qualitative terms, MP2/ADC(2) achieves good agreement with the coupled cluster methods. In both the MP2/ADC(2) calculation and the coupled cluster calculations, the gradient difference vector takes a similar form, and has large components corresponding to bond stretching and bending deformations of the six-membered ring. Insofar as the coupled cluster methods can be considered an accurate benchmark, we may infer that MP2/ADC(2) provides a realistic description of the dependence of the electron binding energy on the molecular geometry.

Figure S1: Gradient difference vector between the D_0 and S_1 (3s) states as calculated with the use of (a) the CCSD and EOM-CCSD methods, and (b) the MP2/ADC(2) methods. The calculations were performed at the chair-equatorial ground-state equilibrium geometry of NMM as optimized at the MP2/r-aug-cc-pVDZ level of theory.

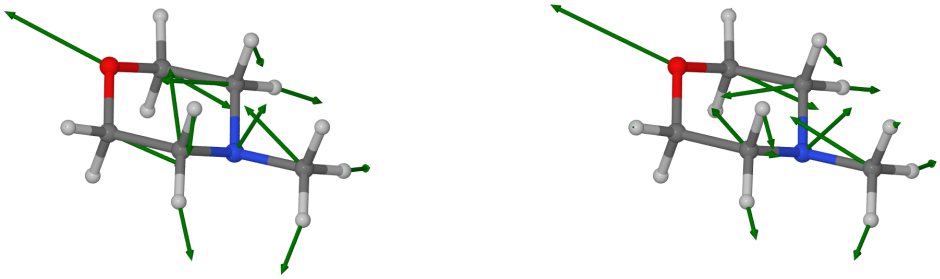

(a) CCSD and EOM-CCSD methods

(b) MP2/ADC(2) method

1.4 Assessment of ADC(2) for ring deformations: normal modes

A reviewer asked the insightful question of how the potential energy surfaces computed with ADC(2) compare to those obtained with EOM-CCSD. In order to answer that question, we performed some additional benchmark calculations.

Firstly, we decided to determine whether ADC(2) provides a realistic decription of the normal modes of the six-membered ring, which are sensitive to the curvature of the potential energy surface. In order to reduce the cost of this calculation, it was performed for the molecule of morpholine, instead of NMM (see the following page for molecular structure). The molecular geometry of the S_1 (3s) state of morpholine was optimized at the MP2/ADC(2)/r-aug-cc-pVDZ level of theory, and at the EOM-CCSD/r-aug-cc-pVDZ level. Subsequently, the normal modes were calculated with the use of the central finite differences method. The simulation setup was the same as in the preceding section. The atomic weights were 1.008 u for hydrogen, 12.011 u for carbon, 14.007 u for nitrogen, and 15.999 u for oxygen.

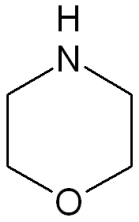

Lewis structure of morpholine

The lowest ten vibrational modes and their frequencies obtained with either method are listed in Table S3. The EOM-CCSD eigenvectors for these modes are illustrated in Figure S2. The vibrational frequencies calculated with MP2/ADC(2) and with EOM-CCSD turn out to coincide closely. This shows that at least in the vicinity of the equilibrium geometry on the S_1 (3s) state, the curvature of the PES provided by MP2/ADC(2) is in good agreement with the higher-level method.

Table S3: Normal modes of morpholine as calculated with the use of the MP2/ADC(2) and EOM-CCSD methods.

Normal mode	Symmetry	Frequency, cm^{-1}	
		MP2/ADC(2)	EOM-CCSD
1	a''	223.9	218.9
2	a'	286.6	266.8
3	a'	389.1	375.9
4	a'	456.5	459.5
5	a''	462.0	468.7
6	a'	524.5	523.5
7	a'	657.0	668.2
8	a''	823.1	824.2
9	a'	852.7	855.2
10	a''	887.2	891.4

Figure S2: Eigenvectors of the lowest ten normal modes of the chair minimum on the S_1 (3s) state of morpholine, as calculated at the EOM-CCSD/r-aug-cc-pVDZ level of theory.

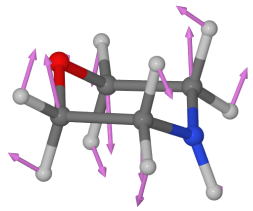

mode 1

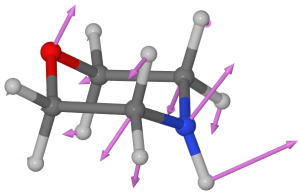

mode 2

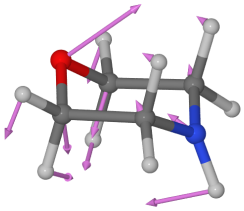

mode 3

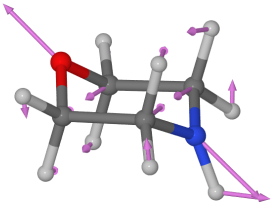

mode 4

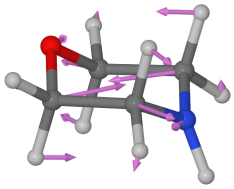

mode 5

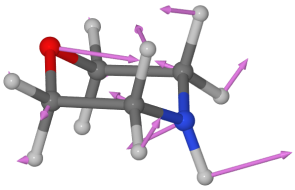

mode 6

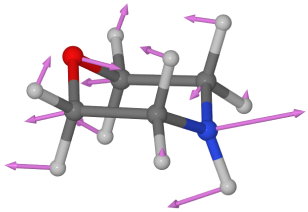

mode 7

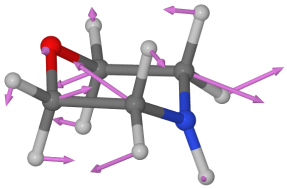

mode 8

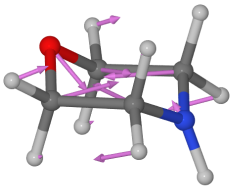

mode 9

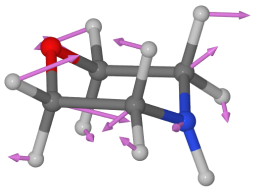

mode 10

1.5 Assessment of ADC(2) for ring deformations: conformational change

In addition to the calculation of the normal modes, it is also interesting to see whether the good performance of MP2/ADC(2) holds up for larger displacements from the equilibrium geometry. To this end, we carried out a potential energy scan of the relevant potential energy surfaces of NMM along a path leading from chair equilibrium geometry on the S_1 (3s) state to the twisted boat equilibrium geometry on that state.

The molecular structures for the purpose of the potential energy surface scan were generated through a linear interpolation in internal coordinates (LIIC) between the chair geometry, and the twisted boat equilibrium geometry. (Both the equilibrium geometries had been previously optimized at the MP2/ADC(2)/r-aug-cc-pVDZ level of theory.) The internal coordinate system used in the interpolation was generated with the use of the `define` utility of Turbomole. As an illustration, selected geometries located along the interpolated path are shown in Figure S3.

In passing, it is worth pointing out that a LIIC path between two geometries does not, in general, coincide within the minimum energy path (MEP) between them. Nevertheless, scanning the energies along the LIIC path should provide a useful indication of the topography of the potential energy surfaces in the intervening region of the configuration space. The setup of the electronic structure calculations was again the same as in Section 1.3.

The results of the potential energy surface scan are shown in Figure S4. For the singlet ground state, MP2 achieves very close agreement with the benchmark provided by the CCSD method.

As stated previously, the MP2/ADC(2) method underestimates the vertical excitation energy into the S_1 (3s) state with respect to the EOM-CCSD method. As a consequence, for the S_1 (3s) state, the potential energy curve obtained with the MP2/ADC(2) method is shifted towards lower energies relative to the curve obtained with the EOM-CCSD method. Apart from that shift, the two curves resemble one another closely. At the EOM-CCSD level, the twisted boat conformer is predicted to be 0.159 eV higher in energy than the chair conformer. At MP2/ADC(2) level, the energy difference is 0.209 eV, meaning that this method achieves satisfactorily good agreement with EOM-CCSD for the relative energies of the two conformers. (Here, the energy difference values are quoted without the inclusion of zero-point vibrational corrections.)

Regarding, in turn, the D_0 state of the $NMM^{\cdot +}$ radical cation, it is once again evident that MP2/ADC(2) underestimates the ionization potential into that state by roughly 0.9 eV with respect to the coupled-cluster method. As a consequence, the potential energy curve obtained with MP2/ADC(2) is downshifted with respect to the curve obtained from coupled-cluster calculations.

As can be seen from Figure S4 (b), the electron binding energy obtained at the MP2/ADC(2) level is underestimated by some 0.5 eV relative to the benchmark value from the coupled-cluster calculations. Aside from this constant shift, it follows the same qualitative trend as in the coupled-cluster calculations.

In summary, although the MP2/ADC(2) method has significant errors for the relative energies of the S_0, S_1 (3s), and D_0 states, these errors appear to be consistent in terms of sign and magnitude. Figuratively speaking, the MP2/ADC(2) shifts the entire potential energy surfaces of the S_1 (3s) and D_0 states downward in energy, the latter more strongly than the former.

Figure S3: Molecular structures located along the LIIC path between the chair equilibrium geometry, and the twisted boat equilibrium geometry, on the S_1 (3s) state of NMM. Structure 0 corresponds the chair equilibrium geometry, while structure 20 is the twisted boat geometry. A total of 19 intermediate structure were generated; this figure only shows every other structure.

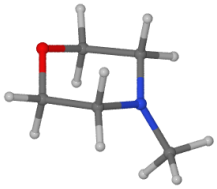

structure 0

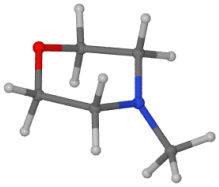

structure 2

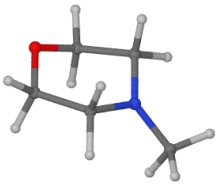

structure 4

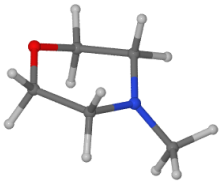

structure 6

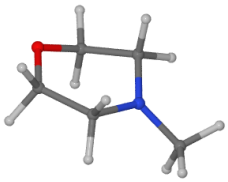

structure 8

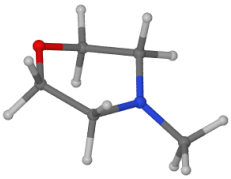

structure 10

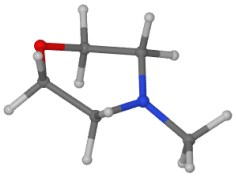

structure 12

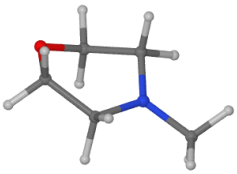

structure 14

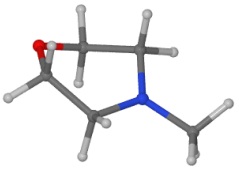

structure 16

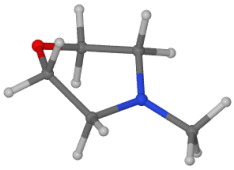

structure 18

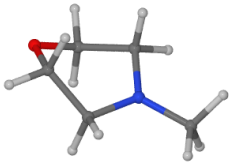

structure 20

Figure S4: Benchmarking the MP2/ADC(2) combination against coupled-cluster (CC) methods for the conformational transition of NMM in its S_1 (3s) state.

(a) Cross-section of the relevant potential energy surfaces of NMM along a LIIC path between the chair equilibrium geometry on the S_1 (3s) state (structure 0), and the twisted boat equilibrium geometry on that state (structure 20). The origin of the potential energy scale corresponds to the energy of the S_0 state at the chair-equatorial ground-state equilibrium geometry.

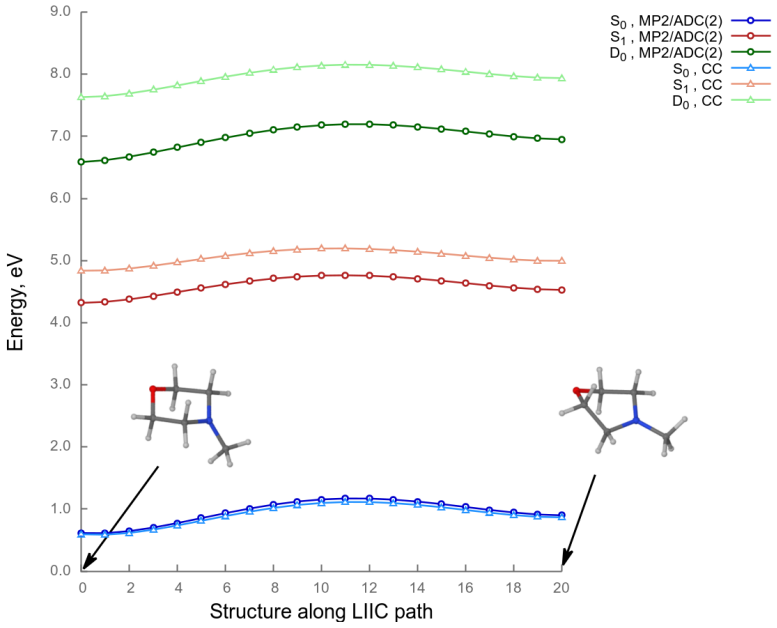

(b) Electron binding energy along the LIIC path.

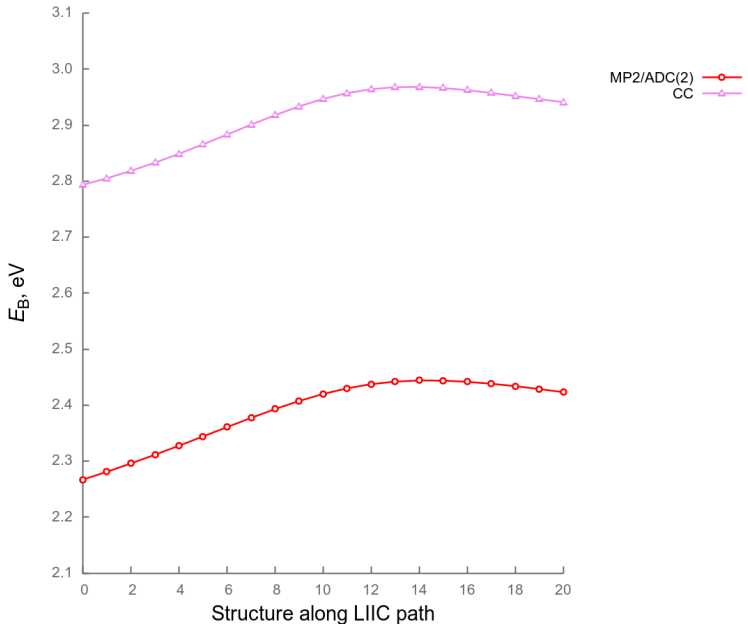

1.6 Outlook

Despite the limited scope of the benchmark calculations described above, some general conclusions may be drawn regarding the applicability of the ADC(2) method for the purpose of simulating TRPES spectra. Clearly, electron binding energies calculated with the use of ADC(2) can be affected by relatively large errors. Whether this represents a serious inaccuracy will depend on the specific problem at hand. In the case of photoionization from Rydberg-type states specifically, the calculation of electron binding energies benefits from favorable error cancellation between the VIP and the vertical excitation energy (ΔE).

In the general case, however, one cannot rely on error cancellation between the VIP and the ΔE. Paradoxically, in the case that ADC(2) does not underestimate the ΔE, its accuracy for the electron binding energy will be worse than if it did. The net conclusion seems to be that ADC(2) is especially well suited for the calculation of the TRPES spectra of aliphatic amines and other molecules whose low-lying excited states are of the Rydberg type. For these systems, the error in electron binding energy should be relatively small and consistent, in terms of sign and magnitude, for all of the relevant excited states. On the other hand, molecules which possess both Rydberg- and valence-type excited states are expected to be more challenging.

2 Definition of parameter Δ

During the analysis of the simulated relaxation dynamics of NMM, we found it useful to construct a parameter which would condense the information provided by the ring puckering coordinates of Hill and Reilly[16] into a single scalar number. We noted, firstly, that at the Franck-Condon geometry, the six-membered ring of NMM is in a chair conformation. What is more, of the two minima on the S_1 (3s) state, the chair minimum is the lower in energy. (See Sections 2.4.1 and 2.4.4 of the main body of the present work.) Accordingly, we decided to define our parameter in such a way as to ensure that it would be sensitive to deviations of the ring geometry from an ideal chair geometry.

To this end, we defined Δ as the distance in the space spanned by θ_0, θ_1, and θ_2, between the current molecular geometry and the ideal $^4C_1$ or $^1C_4$ conformation, whichever is closer:

$$\Delta = \min(\Delta[^4C_1], \Delta[^1C_4]) \tag{4}$$

Here, $\Delta[^4C_1]$ is the distance between the current molecular geometry, and an ideal $^4C_1$ geometry, which is characterized by $\theta_0 = \theta_1 = \theta_2 = 35.26°$:

$$\Delta[^4C_1] = \left[(\theta_0 - 35.26°)^2 + (\theta_1 - 35.26°)^2 + (\theta_2 - 35.26°)^2\right]^{1/2}$$

In turn, $\Delta[^1C_4]$ is the distance between the current molecular geometry, and an ideal $^1C_4$ geometry, which is described by $\theta_0 = \theta_1 = \theta_2 = -35.26°$:

$$\Delta[^1C_4] = \left[(\theta_0 + 35.26°)^2 + (\theta_1 + 35.26°)^2 + (\theta_2 + 35.26°)^2\right]^{1/2}$$

The above definition allows for the fact that during its relaxation dynamics, the molecule may very occasionally 'flip' from a $^4C_1$ conformation to a $^1C_4$ conformation. This is shown schematically in Figure S5. The ring puckering coordinates of Hill and Reilly distinguishes between the two conformations, but for our purposes, they should be treated on an equal footing. Hence, we chose to define Δ as the shorter of the two distances $\Delta[^4C_1]$ and $\Delta[^1C_4]$.

Figure S5: Schematic illustration of the chair conformations $^4C_1$ and $^1C_4$. The two conformations are indistinguishable by means of photoelectron spectroscopy, and for our purposes they should be treated as equivalent. This is taken into account in the definition of parameter Δ.

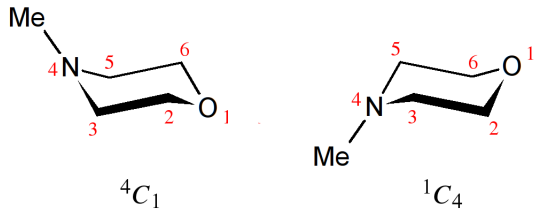

$^4C_1$ $^1C_4$

3 Raw simulated spectrum

As explained in Section 2.3 of the main body of the present paper, the raw simulated TRPES spectrum was treated with a Gaussian blur in the time domain. The goal here was to at least partially account for the various experimental effects which limit the time resolution of the measured TRPES spectrum. In this section, we present the raw simulated spectrum prior to applying the Gaussian blur, as well as the results of applying the blur with a low and a high value of the standard deviation.

Firstly, Figure S6 (a) shows the raw simulated spectrum with no blur. The raw spectrum is somewhat noisy, which complicates attempts at numerical analysis. Most likely, the noisiness is, in part, an artifact of small sample size: the spectrum was calculated on the basis of 38 trajectories, a relatively small number.

As can be seen in Figure S6 (b), the application of a Gaussian blur with a low standard deviation value of $\sigma = 25$ fs reduces the noisiness without obscuring relevant detail: the oscillations in the spectrum.

Lastly, when σ is set to a high value of 75 fs (Figure S6 (c)), the fast oscillations present in the spectrum are smeared out completely. On the other hand, setting σ to 75 fs nicely brings out the 'snaking' appearance of the signal of the 3s state, which is due to the slow oscillation with a period of around 500 fs.

Figure S6: Effects of Gaussian blur in the time domain on the simulated TRPES spectrum. Photoelectron intensity, in arbitrary units, is indicated with the use of color.

(a) raw simulated spectrum with no blur

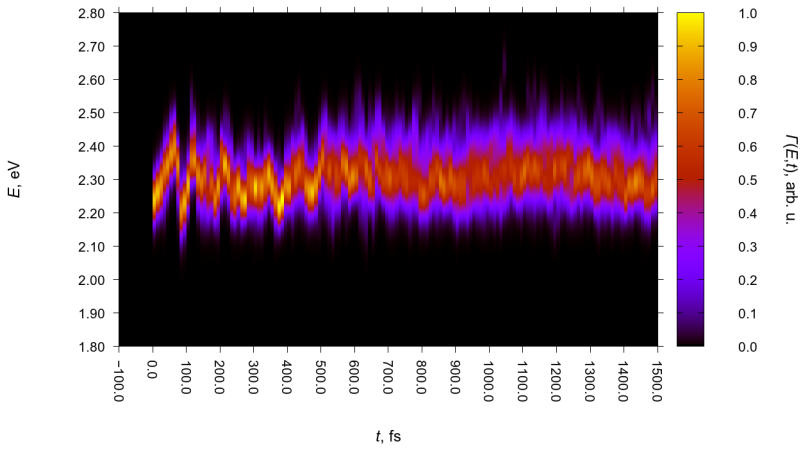

(b) spectrum treated with blur, $\sigma = 25$ fs

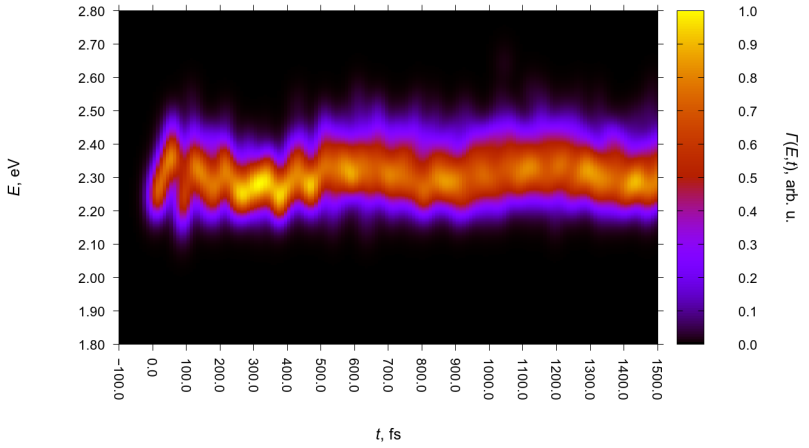

(c) spectrum treated with blur, $\sigma = 75$ fs

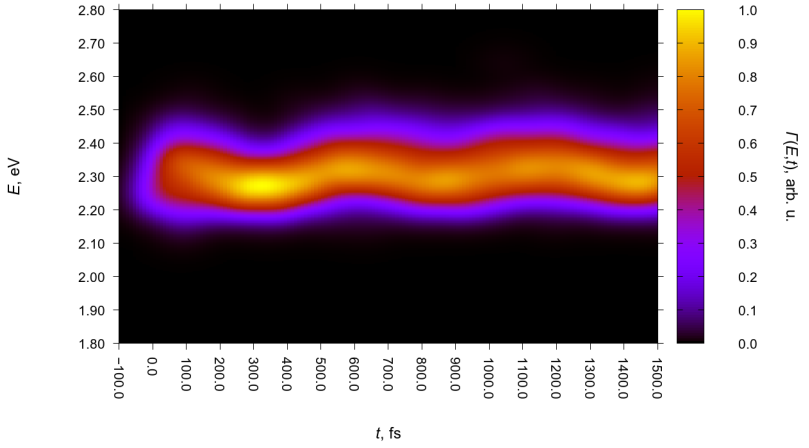

4 Ground-state conformers of NMM

Figure S7 below shows the four ground-state equilibrium geometries of NMM. The simulation setup used during the geometry optimizations is described in Section 2.1 of the main body of the present paper.

Figure S7: The four ground-state equilibrium geometries of NMM, as optimized at the MP2/r-aug-cc-pVDZ level of theory.

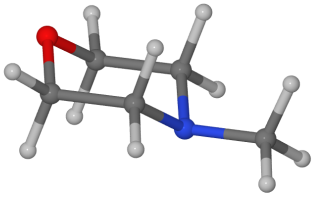

(a) chair-equatorial conformer

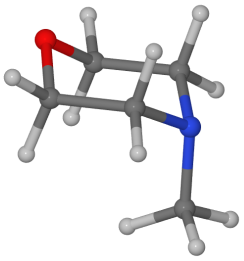

(b) chair-axial conformer

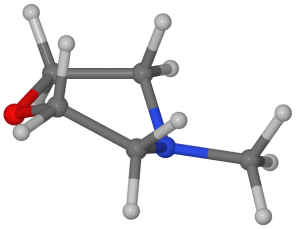

(c) twisted boat-equatorial conformer

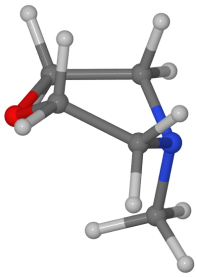

(d) twisted boat-axial conformer

5 Molecular geometries

The present section lists minima on the potential energy surfaces of the S_0 and S_1 (3s) adiabatic states of NMM, as optimized at the MP2/ADC(2)/r-aug-cc-pVDZ level of theory. All geometries are given in terms of Cartesian coordinates in units of ångström (Å).

Moreover, the Supplementary Information includes a ZIP file containing the ensemble of 38 simulated BOMD trajectories. Each individual trajectory is presented in a separate text file in the usual XYZ file format.[17] Snapshots of the molecular geometry are given at intervals of 5 fs starting from the time of the initial photoexcitation (t=0 fs). The trajectories can be viewed with the use of standard visualization programs such as Jmol[18] and GDIS.[19]

Chair equatorial conformer on the S_0 state

C	-1.5082939	0.8557157	-0.0402416
C	-1.5203035	-0.6562355	0.1524234
N	-0.3159681	-1.2412883	-0.4388846
H	-2.4085362	-1.0866294	-0.3438570
H	-1.5875128	-0.8843061	1.2437137
C	0.8606816	-0.6311254	0.1820423
C	0.8215880	0.8802824	-0.0112943
H	1.7698655	-1.0425696	-0.2918656
H	0.9055085	-0.8579926	1.2747308
O	-0.3567247	1.4447197	0.5610905
H	0.8647215	1.1149144	-1.0947829
H	1.6735696	1.3594097	0.4958761
H	-2.3825192	1.3166347	0.4454955
H	-1.5294439	1.0896923	-1.1245239
C	-0.3028747	-2.6892342	-0.2638321
H	-0.3130931	-2.9874572	0.8102755
H	0.6024214	-3.1085094	-0.7329339
H	-1.1871744	-3.1273884	-0.7552019

Chair axial conformer on the S_0 state

C	-1.5145852	0.8831154	-0.0223162
C	-1.5247746	-0.6415533	0.1105662
N	-0.3154295	-1.2820727	-0.4244542
H	-2.4093451	-1.0664375	-0.3971442
H	-1.5931287	-0.8944198	1.1851316
C	0.8662095	-0.6157370	0.1401263
C	0.8263993	0.9083957	0.0066755
H	1.7720208	-1.0212774	-0.3454674
H	0.9134315	-0.8673939	1.2161121
O	-0.3575888	1.4371295	0.6097735
H	0.8724734	1.2186938	-1.0585598
H	1.6760930	1.3688600	0.5364145
H	-2.3868873	1.3249971	0.4860749
H	-1.5409393	1.1926061	-1.0884544
C	-0.2967714	-1.3391023	-1.8856035
H	-1.1790831	-1.9047003	-2.2292647
H	0.6059497	-1.8851078	-2.2072372
H	-0.3012024	-0.3550847	-2.4016709

Twisted boat equatorial conformer on the S_0 state

C	-1.4635170	0.8346667	0.2205062
C	-1.5816240	-0.6724645	-0.0737802
N	-0.2670183	-1.2182023	-0.4373717
H	-2.2780164	-0.8582992	-0.9100761
H	-1.9943881	-1.1754788	0.8337118
C	0.7696806	-0.5261260	0.3168605
C	0.8388392	0.9276937	-0.1820722
H	1.7409835	-1.0175589	0.1362255
H	0.5845297	-0.5710499	1.4176313
O	-0.4451859	1.4260776	-0.5724703
H	1.4656419	0.9893861	-1.0852612
H	1.2763977	1.5772903	0.6039394
H	-1.2577361	1.0073416	1.2968383
H	-2.4024756	1.3529117	-0.0268954
C	-0.2304547	-2.6602472	-0.2420030
H	-1.0361371	-3.1276520	-0.8325397
H	-0.3692260	-2.9525890	0.8254710
H	0.7351183	-3.0597171	-0.5936346

Twisted boat axial conformer on the S_0 state

C	-1.4811476	0.8565998	0.2773094
C	-1.6225429	-0.6518211	-0.0192699
N	-0.3376192	-1.2690587	-0.4015970
H	-2.3367315	-0.8088186	-0.8446058
H	-2.0297122	-1.1625018	0.8759262
C	0.7517303	-0.5317910	0.2367851
C	0.8060098	0.9480674	-0.2113643
H	1.7131614	-1.0269345	0.0141110
H	0.6032417	-0.5984321	1.3297248
O	-0.4931840	1.4306727	-0.5733490
H	1.4278985	1.0742784	-1.1121667
H	1.2364644	1.5773945	0.5963025
H	-1.2123089	1.0298401	1.3402646
H	-2.4235337	1.3912530	0.0792128
C	-0.1616370	-1.3723450	-1.8529678
H	-0.9472796	-2.0288321	-2.2620130
H	0.8130797	-1.8486206	-2.0557946
H	-0.2035575	-0.4018193	-2.3891862

Chair conformer on the S_1 (3s) state

C	-1.5237362	0.6760214	-0.1560163
C	-1.5480904	-0.6637263	0.6307167
N	-0.3106540	-1.3626951	0.3236135
H	-2.4048972	-1.2926759	0.3445956
H	-1.5614935	-0.4524156	1.7131876
C	0.9022809	-0.6120944	0.6054941
C	0.8053252	0.7251104	-0.1800349
H	1.7787879	-1.2044867	0.3016039
H	0.9290004	-0.3997544	1.6875196
O	-0.3706350	1.4182866	0.1895267
H	0.8289568	0.5208823	-1.2663888
H	1.6647325	1.3528728	0.0985298
H	-2.4028791	1.2671816	0.1404674
H	-1.5611244	0.4705296	-1.2417457
C	-0.2954108	-2.5271724	-0.5698067
H	-1.1914603	-3.1342677	-0.3698311
H	0.6313757	-3.0935910	-0.3919281
H	-0.3165969	-2.1524923	-1.6162634

Twisted boat conformer on the S_1 (3s) state

C	-1.4891742	0.8382286	0.5894999
C	-1.6511545	-0.3644067	-0.3323468
N	-0.3259903	-0.8476993	-0.7353984
H	-2.1750342	-0.0975360	-1.2703715
H	-2.1743667	-1.2193177	0.1370376
C	0.8409346	-0.2732896	-0.0724202
C	0.7481330	1.2706712	-0.0616562
H	1.7498302	-0.6317789	-0.5828776
H	0.8252256	-0.6985320	0.9503495
O	-0.5908591	1.7568219	-0.0198592
H	1.1947797	1.6739539	-0.9827495
H	1.3267529	1.6312048	0.8095530
H	-1.1489245	0.5336992	1.5969605
H	-2.4577111	1.3493938	0.6895357
C	-0.1798622	-1.8975475	-1.7453418
H	-1.1765617	-2.2470249	-2.0503691
H	0.4100789	-2.7142057	-1.2965196
H	0.3762371	-1.4555030	-2.5957023

References

[1] Stanton, J. F.; Bartlett, R. J. The Equation of Motion CoupledCluster Method. A Systematic Biorthogonal Approach to Molecular Excitation Energies, Transition Probabilities, and Excited State Properties *J. Chem. Phys.* **1993**, 98, 7029. DOI: 10.1063/1.464746

[2] MOLPRO is a package of *ab initio* programs written by H.-J. Werner, P. J. Knowles, G. Knizia, F. R. Manby, M. Schütz, P. Celani, T. Korona, R. Lindh, A. Mitrushenkov, G. Rauhut, K. R. Shamasundar, T. B. Adler, R. D. Amos, A. Bernhardsson, A. Berning, D. L. Cooper, M. J. O. Deegan, A. J. Dobbyn, F. Eckert, E. Goll, C. Hampel, A. Hesselmann, G. Hetzer, T. Hrenar, G. Jansen, C. Köppl, Y. Liu, A. W. Lloyd, R. A. Mata, A. J. May, S. J. McNicholas, W. Meyer, M. E. Mura, A. Nicklaß, D. P. O'Neill, P. Palmieri, D. Peng, K. Pflüger, R. Pitzer, M. Reiher, T. Shiozaki, H. Stoll, A. J. Stone, R. Tarroni, T. Thorsteinsson, M. Wang. See http://www.molpro.net

[3] Szalay, P. G.; Watson, T.; Perera, A.; Lotrich, V. F.; Bartlett, R. J. Benchmark Studies on the Building Blocks of DNA. 1. Superiority of Coupled Cluster Methods in Describing the Excited States of Nucleobases in the Franck-Condon Region *J. Phys. Chem. A* **2012**, 116, 6702-6710, DOI: 10.1021/jp300977a.

[4] Tajti, A.; Szalay, P. G. Investigation of the Impact of Different Terms in the Second Order Hamiltonian on Excitation Energies of Valence and Rydberg States *J. Chem. Theory Comput.* **2016**, 12, 5477-5482. DOI: 10.1021/acs.jctc.6b00723

[5] Sinha, D.; Mukhopadhyay, S. K.; Chaudhuri, R.; Mukherjee, D. The Eigenvalue-Independent Partitioning Technique in Fock Space: An Alternative Route to Open-Shell Coupled-Cluster Theory for Incomplete Model Spaces *Chem. Phys. Lett.* **1989**, 154, 544-549. DOI: 10.1016/0009-2614(89)87149-0

[6] Stanton, J. F.; Gauss, J. Analytic Energy Derivatives for Ionized States Described by the Equation-of-Motion Coupled Cluster Method *J. Chem. Phys.* **1994**, 101, 8938-8944. DOI: 10.1063/1.468022

[7] Valiev, M.; Bylaska, E. J.; Govind, N.; Kowalski, K.; Straatsma, T. P.; van Dam, H. J. J.; Wang, D.; Nieplocha, J.; Apra, E.; Windus, T. L.; de Jong, W. A. NWChem: a Comprehensive and Scalable Open-Source Solution for Large Scale Molecular Simulations *Comput. Phys. Commun.* **2010**, 181, 1477-1489. 10.1016/j.cpc.2010.04.018

[8] Woon, D. E.; Dunning, T. H. Gaussian Basis Sets for Use in Correlated Molecular Calculations. IV. Calculation of Static Electrical Response Properties *J. Chem. Phys.* **1994**, 100, 2975-2988. DOI: 10.1063/1.466439

[9] Stanton, J. F.; Gauss, J. A Simple Scheme for the Direct Calculation of Ionization Potentials with Coupled-Cluster Theory that Exploits Established Excitation Energy Methods *J. Chem. Phys.* **1999**, 111, 8785-8788, DOI: 10.1063/1.479673.

[10] Neville, S. P.; Averbukh, V.; Patchkovskii, S.; Ruberti, M.; Yun, R.; Chergui, M.; Stolow, A.; Schuurman, M. S. Beyond Structure: Ultrafast X-ray Absorption Spectroscopy as a Probe of Non-adiabatic Wavepacket Dynamics *Faraday Discuss.* **2016**, 194, 117-145. DOI: 10.1039/c6fd00117c

[11] Christiansen, O.; Koch, H.; Jørgensen, P. The Second-Order Approximate Coupled Cluster Singles and Doubles Model CC2 *Chem. Phys. Lett.* **1995**, 243, 409-418, DOI: 10.1016/0009-2614(95)00841-Q

[12] Hättig, C. Structure Optimizations for Excited States with Correlated Second-Order Methods: CC2 and ADC(2). In *Advances in Quantum Chemistry*; Jensen, H. J. Å.., Ed.; Academic Press: New York, 2005; Vol. 50; pp 37-60. DOI: 10.1016/S0065-3276(05)50003-0

[13] Hohenstein, E. G.; Kokkila, S. I. L.; Parrish, R. M.; Martínez, T. J. Tensor Hypercontraction Equation-of-Motion Second-Order Approximate Coupled Cluster: Electronic Excitation Energies in $\mathcal{O}(N^4)$ Time *J. Phys. Chem. B* **2013**, 117, 12972-12978, DOI: 10.1021/jp4021905

[14] Head-Gordon, M.; Oumi, M.; Maurice, D. Quasidegenerate Second-Order Perturbation Corrections to Single-Excitation Configuration Interaction *Mol. Phys.* **1999**, 96, 593-602. DOI: 10.1080/00268979909482996

[15] Turney, J. M.; Simmonett, A. C.; Parrish, R. M.; Hohenstein, E. G.; Evangelista, F. A.; Fermann, J. T.; Mintz, B. J.; Burns, L. A.; Wilke, J. J.; Abrams, M. L.; Russ, N. J.; Leininger, M. L.; Janssen, C. L.; Seidl, E. T.; Allen, W. D.; Schaefer, H. F.; King, R. A.; Valeev, E. F.; Sherrill, C. D.; Crawford, T. D. PSI4: an Open-Source *Ab Initio* Electronic Structure Program *WIREs Comput. Mol. Sci.* **2012**, 2, 556-565.

[16] Hill, A. D.; Reilly, P. J. Puckering Coordinates of Monocyclic Rings by Triangular Decomposition *J. Chem. Inf. Model.* **2007**, 47, 1031-1035. DOI: 10.1021/ci600492e

[17] https://en.wikipedia.org/wiki/XYZ_file_format

[18] Jmol: an open-source Java viewer for chemical structures in 3D. http://www.jmol.org/

[19] GDIS is a GTK based program for the display and manipulation of isolated molecules and periodic systems. http://gdis.seul.org/